Songklanakarin J. Sci. Technol.
39 (6), 793-801, Nov. - Dec. 2017

http://www.sjst.psu.ac.th

Original Article

3D plane cuts and cubic Bézier curve for CT liver volume segmentation according to Couinaud's classification

Chitsanupong Butdee[1], Charnchai Pluempitiwiriyawej[2]*, and Natthaporn Tanpowpong[3]

[1] *Biomedical Engineering Program, Faculty of Engineering, Chulalongkorn University, Pathum Wan, Bangkok, 10330 Thailand*

[2] *Department of Electrical Engineering, Faculty of Engineering, Chulalongkorn University, Pathum Wan, Bangkok, 10330 Thailand*

[3] *Department of Radiology, Faculty of Medicine, Chulalongkorn University, Pathum Wan, Bangkok, 10330 Thailand*

Received: 21 May 2016; Revised: 15 September 2016; Accepted: 19 September 2016

Abstract

In pre-operative planning for partial liver transplantation, the total liver volume must be virtually segmented from a set of CT scanned images. The liver, consequently, is divided into eight segments according to Couinaud's classification using hepatic and portal veins as clues. To facilitate the visualization of the segmented liver model, we propose a computerized process using four 3D plane cuts and cubic Bézier curve. In our experiments, fifteen liver volumes were used, and each of them was cut into eight segments using our program and their average percentage volumes were analyzed. The results were in agreement with the ground truth. Our program is semi-automatic. It requires minimal user interactions. As a result, the user can easily view the segmented liver model in both 2D and 3D perspectives.

Keywords: liver segmentation, Couinaud's classification, 3D region growing, Bézier curve, 3D plane cuts

1. Introduction

Liver transplantation is the implantation of a new normal liver tissue to a patient who has chronic abnormal liver function. The source of the transplanted liver is usually a donor who has just passed away. Recently, however, a living donor can also donate a part of his/her normal liver to a patient for partial liver transplantation. The question of how much liver volume should be donated to the patient arises. The donated liver part should have enough volume to provide new liver function for the patient whilst retaining about 35% to 40% of the original liver volume for the correct functioning in the living donor (Suzuki *et al.,* 2010). Therefore, an accurate assessment of liver volume segmentation is essential for pre-operative planning.

Due to its high resolution and low cost, computed tomography (CT) is one of the imaging modalities that is widely used to capture the anatomy of the liver. In a regular pre-operative procedure, the liver is first manually segmented in a sequence of cross-sectional CT scans, then its volume is further divided into eight sub-segments according to Couinaud's classification (Rutkauskas *et al.,* 2006) using branches of the hepatic and portal veins as clues. Although segmentation of the whole liver could be done manually on two-dimensional (2D) cross-sectional images slice by slice, further segment the liver volumes into eight sub-segments according to Couinaud's classification is impractical because it mostly requires three-dimensional (3D) visualization.

* Corresponding author.
Email address: charnchai.p@chula.ac.th

Therefore, we propose a computerized method to perform the task using 3D plane cuts and cubic Bézier curve (Masood & Ejaz, 2010) using clues from hepatic and portal veins.

There are many reports on computerized whole liver segmentation. Gao *et al.* (1996) used thresholding and morphological operation. Xu *et al.* (2010) used the local entropy method to delineate the liver boundary and the tumor within it. Liu *et al.* (2005) used the gradient vector flow (GVF) snake with an improved edge map. Badakhshannoory and Saeedi (2011) used the principle component analysis (PCA) to segment the kidney and liver in each 2D image slice, and then the results were combined to form a 3D liver volume. Abdel-massieh *et al.* (2010) used a statistical model in the first part of their liver segmentation, followed by an active contour to refine the segmented result.

Lesage *et al.* (2009) published an extensive literature review on vessel segmentation. Some interesting techniques are 3D multi-scale line filter by Sato *et al*. (1998) and a locally adaptive region growing algorithm by Yi & Ra (2003). More recently, Jiang *et al.* (2013) proposed a spectrum based region growing and 3D reconstruction to segment optical and hepatic vessels.

For reports on segmentation of the whole liver into eight Couinaud sub-segments, we found only a few. Haung *et al*. (2008) projected 3D segmented liver and veins onto two planes, then a 2D quadratic curve fitting was applied to approximate the curve planes that divided the liver into seven Couinaud sub-segments, where the first Couinaud sub-segment or the Caudate lobe was not segmented out. It was blended as a part of other segments. Oliveira *et al.* (2011) used least square method to obtain four planes to cut the whole liver. We observed that the caudate lobe was not segmented.

In this paper, we propose a computerized process with minimal user interaction that can segment the whole liver volume, as well as the hepatic and portal veins, and then divide the liver volume into eight segments according to Couinaud's classification. The program uses a 3D region growing algorithm to segment the whole 3D liver volume and the veins. To obtain eight Couinaud sub-segments, first, a set of cubic Bézier curves are generated to segment the caudate lobe out, and then four 3D planes are formed by geometric approach to divide the liver into other seven segments.

2. Materials and Methods

2.1 Dataset

Abdominal CT scans of 15 living donors were used to test our program. A contrast agent was administrated into the portal venous phase of the scan. Each obtained DICOM image had a size of 512 x 512 pixels, with slice thickness between 2.5 and 6 mm.

This study had been ethically reviewed by the research affairs committee, Faculty of Medicine, Chulalongkorn University. All algorithms were implemented using MATLAB on an Intel® Xeon ® CPU x 3450 at 2.67 GHz,.

2.2 Algorithms

Our proposed program consists of (1) 3D liver volume segmentation out of a set of CT scans, (2) portal and hepatic vessel segmentation, and (3) segmentation of the liver volume into eight segments. Manual segmentation by a radiologist is used as a 'ground truth' for comparison of total liver volume segmentation.

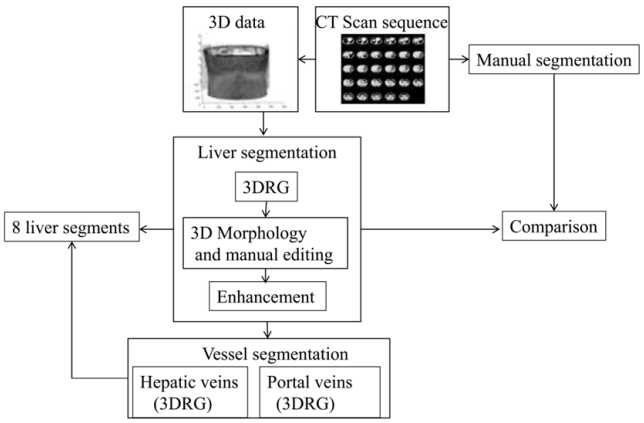

Figure 1. Flowchart of our program

Figure 1 shows the flowchart of the algorithms used in our program. Starting with a sequence of 2D cross-sectional scans of an abdomen, a 3D dataset was formed. For 3D liver segmentation, 3D region growing algorithm is applied. The result is a 3D binary volume representing the liver part. To refine the segmented result, 3D morphological processing is used. The 3D binary liver volume is then used as a mask on the original gray-scale image dataset to show only the liver part of the data. Enhancement is applied for a better visualization of the area within the liver region. Consequently, the enhanced liver volume is used as an input to 3D region growing algorithm two more times, once to segment the hepatic veins, and then next to segment the portal vein. Finally, the information about the hepatic and portal veins is superimposed onto the liver volume and the images of all liver slices are shown to the user, in this case a radiologist, so they can conveniently choose points that will be used to form plane cuts that will divide the 3D liver volume into eight segments according to Couinaud's classification.

2.2.1 Pre-processing step

In this step, the cross sectional CT scan of some 29-88 slices are stacked to form a 3D data and the Gaussian filter is applied for noise reduction

2.2.2 Liver segmentation

We chose a region growing algorithm, which is a region based method for image segmentation. Starting from

a seed pixel within the liver tissue, the algorithm checks the intensity value of the neighboring pixels then expands the object region gradually if they have similar intensity values within a pre-set range. A pixel is classified as an object pixel according to not only its intensity relative to the existing object's intensity but also its connectivity to the existing object region. Otherwise, it is considered a background pixel. The region growing algorithm will stop when all pixels within the image have been investigated and classified as either the object or the background. The neighboring pixels are pixels adjacent to the object region. For 3D region growing, we used 6-connected neighboring pixels. In addition to the 4-connected pixels in the same image slice, we also checked for 2 more connected pixels at the top and the bottom slices. To start the process, the user selected the slice with the largest liver tissue area and picked only one seed point within the liver tissue area. Then a small cube around the selected seed point was formed and standard deviation (SD) of intensity values of the pixels within the cube was calculated. The pre-set range was set at the intensity value of the initial seed ±10% of the SD.

After the 3D region growing algorithm had been applied to the image data set, we found that the resulting liver region might include more than just the actual liver pixels. Removal of extraneous regions was therefore sometimes necessary, so we needed to apply 3D morphological opening & closing filters to remove any protruding or intruding noisy parts of the liver volume. After the morphological operations were applied, the expected liver volume should appear as one single region. However, we found that our resulting 3D binary volume showed more than one region. Therefore, a search for the connected components was needed and we chose the largest 3D connected component as our refined liver region. At this point, if parts of other neighboring organs such as heart, kidney, spleen or pancreas were still included in our automatic liver segmentation so far, some manual editing would be necessary. Nonetheless manually deselecting of these other organs at this final step is much simpler than delineating the liver boundary in each image slice manually from the beginning. Finally, the liver volume was calculated and the results of the computer assisted liver segmentation were compared to the ground truth data, which was the manual segmentation by an expert without any computerized image processing.

2.2.3 Vessel segmentation

Segmentations of the hepatic and portal veins are also necessary because the surgeons need them as a reference for alignment when dividing the liver volume into the eight sub-segments according to Couinaud's classification. To remove just a part of the whole liver, the surgeons usually cut the liver along the border of the liver's sub-segment to avoid any damage to the remaining liver, thus allowing the donors to retain the remaining liver functioning in their body.

To extract the hepatic and portal veins from our 3D image data set via the 3D region growing algorithm, two seed points were selected, one at a time, within each vein area. We first super-imposed the obtained binary liver mask onto the original image data set to show the gray scale image of only the liver region in each slice. Some enhancement of the gray values may be necessary for optimal visualization. Then a pixel within the hepatic vein in any slice was selected as a seed point for the 3D region growing algorithm to trace the hepatic vein. In our case, the seed point was selected at the main branch of the hepatic vein. The same process was repeated for segmentation of the portal vein.

This venous information provided clues for the user to conveniently select points necessary for creating the curve and planes used in the segmentation process of the liver volume. Since it was difficult to visually select points in the 3D space on the computer screen, we designed the program for the user to select points from 2D cross-sectional images at different slices and then transfer their locations into points in the 3D space. Figure 2 shows branches of the hepatic vein (in red) and of the portal vein (in blue) overlaid onto gray scale liver slices.

2.2.4 Liver sub-segment

The information about the liver volume and its vessels, i.e., hepatic and portal veins, was used in the process of dividing the liver into the eight segments. Our algorithm cuts the liver using a cubic Bézier curve and four 3D planes. The Bézier curve is to extract the caudate lobe (segment I) at the core connecting the upper and lower portions of the liver. Four 3D planes are then used to divide the remaining liver volume. They consist of three vertical planes along the middle, left, and right branches of the hepatic veins and one transverse plane along the portal vein. The transverse plane divides the liver volume into the upper and the lower parts. The vertical plane along the middle hepatic vein divides the liver volume into left and right lobes. The left hepatic lobe is

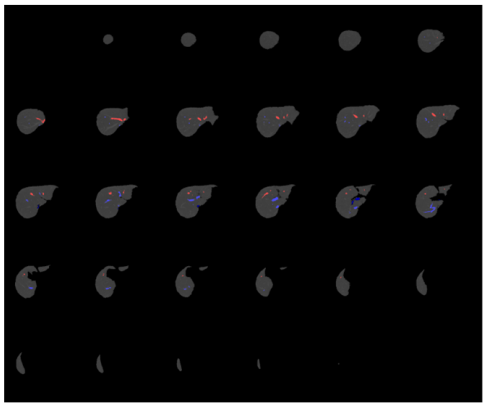

Figure 2. The RGB colors of hepatic (red) and portal (blue) veins overlaid on the gray scale image of liver volume.

further cut by the plane along the left hepatic vein resulting in the medial and lateral segments. Similarly, the right hepatic lobe cut by the plane along the right hepatic vein results in the anterior and posterior segments. In the segmentation of the caudate lobe, a cubic Bézier curve according to equation (1) is used.

$$B(t) = (1-t)^3 P_0 + 3(1-t)^2 tP_1 + 3(1-t)t^3 P_2 + t^3 P_3, t \in [0,1] \quad (1)$$

where P_0, P_1, P_2, P_3 are 4 controlling points, and t is the curve parameter necessary to form a cubic Bézier curve. In Figure 3(a), four points on the liver slice with the largest caudate area (usually the middle slice) are chosen and a cubic Bézier curve is formed. Figure 3(b) depicts the area within the cubic Bézier curve, which is used as a mask for the caudate region in such liver slice. The caudate regions in other adjacent slices are then automatically generated by interpolating the caudate mask in the slice up and down with a scaling factor defined as in equation (2).

$$Q = \frac{(\alpha - 1)k}{ss} + 1, \quad (2)$$

where ss is the number of slices to be interpolated up or down, the parameter k takes an integer value from 1 to ss, the parameter α has a value in the range from 0 to 1, representing the final scaling factor at the ending slice. The user will specify two values for ss, one for the number of slices to be interpolated up and the other for the number of slices to be interpolated down. With this equation, the caudate region in each interpolated slice will be gradually reduced as shown in Figure 4(a). The number of slices to be interpolated up, ss is 5 and the values for k are from 1 to 5 for each slice in ascending order. On the other hand, the number of slices to be interpolated down, ss is 4 and the values for k are from 1 to 4 for each slice in descending order, resulting in gradually smaller caudate region in five slices above and four slice below the initially drawn slice, respectively as shown in Figure 4(b).

(a) (b)

Figure 3 (a) outline of cubic Bézier curve using 4 control points (b) mask of the Bézier curve the segmented result and use as mask interpolate by scaling factor for other slices.

To create a 3D plane, three non-linearly aligned points are necessary. Suppose the three points that define a plane in 3D space have been chosen as, $A(x_0, y_0, z_0)$, $B(x_1, y_1, z_1)$, $C(x_2, y_2, z_2)$. Two vectors AB and AC can be formed following equations (3) and (4). The cross product of the two vectors is then computed, in equation (5), to form the normal vector (the vector perpendicular) to the desired plane. Using the coefficients a, b, and c of the normal vector and any point on the plane, in this case we use $A(x_0, y_0, z_0)$, the equation for the plane can be formed as equation (6). Consequently, equation (7) is simply equation (6) normalized by a factor of $ax_0 + by_0 + cz_0$.

$$\overrightarrow{AB} = (x_1 - x_0)\hat{i} + (y_1 - y_0)\hat{j} + (z_1 - z_0)\hat{k} \quad (3)$$

$$\overrightarrow{AC} = (x_2 - x_0)\hat{i} + (y_2 - y_0)\hat{j} + (z_2 - z_0)\hat{k} \quad (4)$$

$$\overrightarrow{AB} \times \overrightarrow{AC} = \begin{vmatrix} \hat{i} & \hat{j} & \hat{k} \\ (x_1 - x_0) & (y_1 - y_0) & (z_1 - z_0) \\ (x_2 - x_0) & (y_2 - y_0) & (z_2 - z_0) \end{vmatrix} = a\hat{i} + b\hat{j} + c\hat{k} \quad (5)$$

$$a(x - x_0) + b(y - y_0) + c(z - z_0) = 0 \quad (6)$$

$$\bar{a}x + \bar{b}y + \bar{c}z - 1 = 0 \quad (7)$$

Finally, the plane equation (7) is used to divide the 3D data points into 2 groups by changing equation (7) into

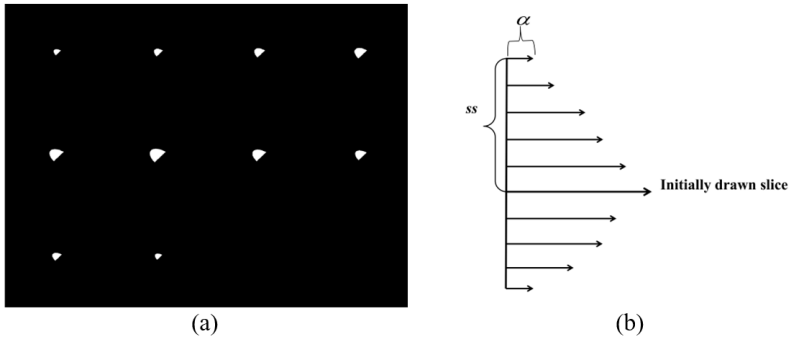

(a) (b)

Figure 4. (a) shows the cross-sectional view of the caudate regions in each liver slice above and below the initially drawn slice (b) depicts the corresponding coronal views showing relative scaling in each slice with respect to the initially drawn slice.

inequalities. The first group consists of any point that makes the equation result greater than zero. On the other hand, those points in 3D space that change equation (7) result to be less than zero are on the other side of the plane. Branches of the hepatic vein at different slices of the liver volume are used as clues in point selections. Currently they are selected manually by the user. To accelerate the process, however, the selection of points can be made automatic.

Theoretically, 9 points are necessary to create three vertical planes: the first plane along the direction of the middle hepatic, the second one along the right hepatic vein, and the third one along the left hepatic vein. These 3 planes, however, usually have one common point at the inferior vena cava. Therefore, only 7 points are needed.

For the transverse plane that divides the liver volume into the upper and the lower parts, the user only needs to choose one image slice with the most visible portal vein area. As a result, the liver volume will be divided into the upper portion comprising segments II, IVa, V, VIII, and the lower part comprising segments III, IVb, VI, and VII. together with segment I (the caudate); eight segments of the liver volume according to Couinaud's classification.

The results of our liver segmentation by 3D region growing are compared to the manual segmentation using the dice similarity (DS), the false positive ratio (FPR) and the false negative ratio (FNR) (Bartnykas, 2010) followings equations (8), (9) and (10), respectively. For the 3D data set, we compare them in terms of image volume. The dice similarity finds the matched liver voxels in both liver volumes. Therefore, if both volumes are a perfect match, the value for DS would be 100%. The FPR counts the number of background voxels that are classified as the liver voxels. On the other hand, the FNR indicates the proportion of the liver voxels that are misclassified as the background. We expect these two misclassification errors to be small.

$$DS = 2\frac{|C_L \cap M_L|}{|C_L| + |M_L|} x100\%, \quad (8)$$

$$FPR = 2\frac{|C_L \cap M_B|}{|C_L| + |M_L|} x100\%, \quad (9)$$

$$FNR = 2\frac{|C_B \cap M_L|}{|C_B| + |M_L|} x100\%, \quad (10)$$

where
C_L is the liver volume segmented by computer,
C_B is the background volume segmented by computer,
M_L is the liver volume segmented manually,
M_B is the background volume segmented manually.

Finally, we compare the computerized liver volume with the manually segmented liver volume through percent volume error (PVE) (Hori *et al.*, 2011) as in equation (11). The positive value for PVE indicates that the computerized liver volume is larger than the ground truth; whereas the negative value shows an under segmentation.

$$PVE = \frac{C_{Vol} - M_{Vol}}{M_{Vol}} \times 100\% \quad (11)$$

where
C_{Vol} is the liver volume segmented by computer,
M_{Vol} is the liver volume segmented manually

3. Results and Discussion

Table 1 shows the comparison of 15 liver volumes segmented by our computer program with the ground truth segmented manually by an expert. We can see that all of them have better than 94% similarity to the ground truth with some errors between 1.8% and 6.7%. Twelve out of fifteen are under-segmented. The average values for DS, FPR, FNR and PVE are 96.1%, 3.4%, 4.4% and - 0.1%, respectively.

The 3D display of a liver volume segmentation result is shown in Figure 5(a). The hepatic and portal veins segmentations displayed within the transparent liver volume are shown in Figure 5(b). Furthermore, the 15 liver volumes are divided into eight segments by a drawing of the cubic Bézier curve and 7 points selected for the creation of 3D planes along the hepatic main branches and portal veins as described earlier. The volumes of each segment in each liver are shown in Table 2 and the average time required in this process is about 46 seconds as shown in Table 3.

Figure 6(a) and 6(b) illustrate two different views as an example of the 3D display of the segmentation of the liver volume according to Couinaud's classification with different color representation of the different segments. Figure 7 depicts the corresponding 2D display in RGB colors for each segment overlaid on 2D gray scale cross sectional image slices. It shows alignments of each 3D plane that cut the liver volume into eight segments

Table 1. Comparison of the liver volume segmented by our computer program to the ground truth.

Data	DS (%)	FPR (%)	FNR (%)	PVE (%)
1	96.9	2.4	3.7	-1.2
2	95.9	4.0	4.3	-0.3
3	94.5	3.6	6.5	-2.8
4	95.5	4.2	4.8	-0.6
5	97.2	3.8	1.8	2.0
6	95.9	2.7	5.5	-2.8
7	96.8	4.4	1.9	2.4
8	96.3	5.5	1.9	3.8
9	95.8	1.8	6.7	-4.8
10	95.7	2.4	6.1	-3.6
11	96.2	2.4	5.3	-2.8
12	94.9	3.9	6.3	-2.3
13	97.2	2.2	3.5	-1.3
14	95.7	4.2	4.5	-0.3
15	96.4	3.5	3.7	-0.2
Average	96.1	3.4	4.4	-1.0

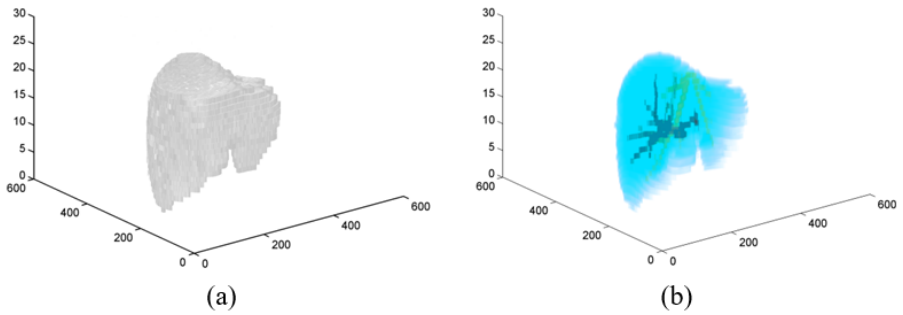

Figure 5. (a) Segmented 3D liver volume by 3D-RG algorithm (b) 3D liver with transparency, the hepatic vein show in yellow and portal vein in blue.

Table 2. Segments of the liver volume according to Couinaud's classification and their volume percentage

Data	Total volume	Seg.I (cm^3)	Seg.II (cm^3)	Seg.III (cm^3)	Seg.IV (cm^3)	Seg.V (cm^3)	Seg.VI (cm^3)	Seg.VII (cm^3)	Seg.VIII (cm^3)
1	1323.8	37.0	163.6	68.8	327.7	200.0	149.2	211.1	171.6
	100.0%	2.4%	12.4%	5.2%	24.8%	15.1%	11.3%	15.9%	13.0%
2	1451.1	36.42.5%	96.9	71.9	300.7	221.3	237.3	285.2	201.4
	100.0%	6.7%	5.0%	20.7%	15.3%	16.4%	19.7%	13.9%	
3	1437.9	28.1	205.9	33.1	253.8	257.3	180.4	212.7	266.6
	100.0%	2.0%	14.3%	2.3%	17.7%	17.9%	12.5%	14.8%	18.5%
4	1656.6	35.3	161.3	98.4	356.7	145.3	259.1	244.3	356.3
	100.0%	2.1%	9.7%	5.9%	21.5%	8.8%	15.6%	14.7%	21.5%
5	1361.7	27.5	207.0	61.1	165.0	70.0	333.3	102.4	395.3
	100.0%	2.0%	15.2%	4.5%	12.1%	5.1%	24.5%	7.5%	29.0%
6	1459.1	31.4	244.8	85.4	292.0	121.7	279.5	163.8	240.5
	100.0%	2.2%	16.8%	5.8%	20.0%	8.3%	19.2%	11.2%	16.5%
7	1317.7	25.9	165.5	93.3	214.8	199.4	236.7	198.8	183.3
	100.0%	2.0%	12.6%	7.1%	16.3%	15.1%	18.0%	15.1%	13.9%
8	1338.1	22.4	158.8	17.9	440.4	47.0	326.8	56.1	268.8
	100.0%	1.7%	11.9%	1.3%	32.9%	3.5%	24.4%	4.2%	20.1%
9	1223.3	18.7	134.5	83.5	220.4	124.6	228.6	163.5	249.6
	100%	1.5%	11.0%	6.8%	18.0%	10.2%	18.7%	13.4%	20.4%
10	1052.5	15.9	126.8	68.3	179.1	87.7	276.6	76.0	222.0
	100.0%	1.5%	12.1%	6.5%	17.0%	8.3%	26.3%	7.2%	21.1%
11	1001.5	29.9	136.1	49.5	211.1	182.0	147.4	136.5	109.1
	100.0%	3.0%	13.6%	4.9%	21.1%	18.2%	14.7%	13.6%	10.9%
12	849.2	15.0	110.9	21.3	175.1	162.5	176.9	78.4	109.3
	100.0%	1.8%	13.1%	2.5%	20.6%	19.1%	20.8%	9.2%	12.9%
13	1559.8	19.4	227.4	12.1	330.3	124.9	339.5	114.5	391.7
	100.0%	1.2%	14.6%	0.8%	21.2%	8.0%	21.8%	7.3%	25.1%
14	1340.4	24.6	187.5	97.2	110.8	165.2	229.7	278.9	246.6
	100.0%	1.8%	14.0%	7.2%	8.3%	12.3%	17.1%	20.8%	18.4%
15	1346.3	19.5	239.4	88.2	417.4	78.2	228.7	74.8	200.2
	100.0%	1.4%	17.8%	6.6%	31.0%	5.8%	17.0%	5.6%	14.9%
Average	1314.6	25.8	171.1	63.3	266.4	145.8	242.0	179.8	240.8
	100.0%	1.9%	13.1%	4.8%	20.2%	11.4%	18.6%	12.0%	18.0%

The liver volumes were segmented and compared with the ground truth using DS, FPR, PNR, and PVE. The DS value should be more than 70%, the FPR and FNR value should below 5%, imply good agreement between two segmentation results as suggested in Bartnykas (2010). In this work on multifraction analysis, only two datasets were used. The DS are 82.7±6.9% and 95.8±1.7% The FPR are 5.9±8.9% and 4.6±2%. The FNR are 28.9±19% and 3.8±3.3% for the first

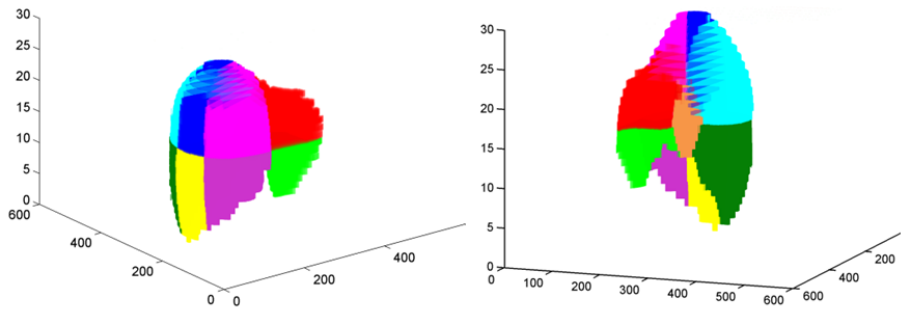

Figure 6. The 3D display of the resulted liver segments according to Couinaud's classification: the Segment I show in orange, the segment II in red, the segment III in light green, the segment IV in purple, the segment V in yellow, the segment VI in dark green, the segment VII in cyan, the segment VIII in blue.

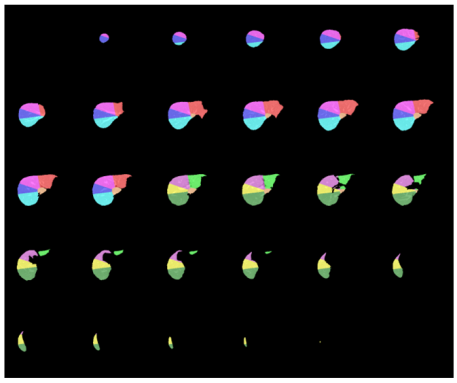

Figure 7. The 2D display of all slices of the resulted liver segments according to Couinaud's classification.

and second datasets, respectively. In our experiments, the DS measures are within the 94.5-97.2% range, which is much more than 70%. The FPR values are between 1.8-5.5% with an average FPR of 3.4% and the FNR values are in the 1.8-6.7% range with an average FNR of 4.4%, which is slightly more than the FPR, this leads to under-segmentations. Furthermore, the PVE is also used to validate our segmentation results to the ground truth. Most of the resulting PVE values are negative, implying that most liver volumes segmented by the computer are smaller in size than the manual segmentation. Such under-segmented results are due to the inhomogeneous intensity of the liver region across each slice. The intensity of the pixels within the liver region in the top slices is usually less than that of the liver region in the bottom slices. As a result, the liver region in the top slice is often missed. Suzuki *et al.* (2010) used Geodesic active contour coupled with level set algorithm to segment liver from 4 datasets, the average PVE was 7.2%.

As for the segmentation of the hepatic and portal veins, we also use 3D RG algorithm with seed values within the main branches of the hepatic and portal veins. Since the pixel intensities within each vein may not be homogeneous within the entire vessel, the 3D RG algorithm can only trace areas near the main branches, and may not be able to trace the ends of their branches. We cannot set the preset range of the algorithm to cover a large range of intensity values, or else it is quite easy to leak into the liver tissue. However, the main branch information is enough for the computer's point selection process to create 3D planes because the user only considers points within the main branches.

Finally, our computer program also cut the liver volume into eight segments according to Couinaud's classification by manually choosing 7 points within the main hepatic and portal braches to automatically create 4 planes (3 vertical planes and one transverse plane) and manually tracing the caudate lobe from 6 points selected by the cubic Bézier curve. The results are illustrated in both 3D display (as in Figure 6) and the 2D RGB color overlaid on the cross-sectional gray scale image slices (as in Figure 7) for visual evaluation. In addition, the percentage volumes of all segments are summarized in Table 2. The processing time for each step is summarized in Table 3. The results revealed that the average values of proposed method with manual editing and manual segmentation only were 51 and 55 minutes, respectively, implying that our algorithm is better than the total manual segmentation by about 8%. The most of image datasets, our 3DRG + 3D morphology algorithm facilitate the manual editing task to perform faster than the total manual segmentation alone.

4. Conclusions

We segmented the 3D liver volume from 15 sets of CT cross-sectional liver scans. Boundaries of the whole liver surface were extracted using a 3D region growing algorithm and compared to the ground truth. The algorithm showed about 96.1% accuracy. Most of the results were under-segmented, with percentage total liver volume difference about -1%. Furthermore, the portal and hepatic veins were also segmented and used as clues to form 3D-plane-cuts and

Table 3. The whole liver segmentation by our proposed method compared to the processing time of total manual segmentation by an expert and processing time of liver sub-segments

Data	3DRG and 3D morphology (minutes)	Manual editing (minutes)	The proposed method with manual editing (minutes)	Manual segmentation (minutes)	Liver sub-segment (seconds)
1	4	14	18	20	47
2	4	20	24	34	31
3	5	40	45	62	48
4	8	44	52	66	47
5	5	60	65	75	43
6	11	52	63	82	41
7	11	34	45	48	63
8	5	37	42	42	44
9	3	35	38	39	37
10	7	38	45	52	44
11	8	45	53	45	59
12	4	48	52	53	50
13	10	60	70	75	48
14	19	68	87	70	45
15	7	52	59	59	44
Average	7	43	51	55	46

cubic Bézier curve for dividing the liver into eight sub-segments. The total liver volume and liver sub-segment volumes can be automatically calculated via algorithm. In the case of partial liver transplantation, in particular, the remaining liver volume can be estimated. This could facilitate a surgeon in making a decision on how much liver volume a living donor can donate a part of his/her normal liver to a patient for pre-operative planning in the future.

Acknowledgements

We would like to thank King Chulalongkorn Memorial Hospital for providing abdominal CT scan image datasets. We would like to thank THE 90TH ANNIVERSARY OF CHULALONGKORN UNIVERSITY FUND for financial support and many thanks to Mr. Roy Morien of the Naresuan University Language Centre for his advising on English expression in this document.

References

Abdel-massieh, N. H., Hadhoud, M. M., & Moustafa, K. A. (2010, March). *A fully automatic and efficient technique for liver segmentation from abdominal CT images.* Paper presented at the 7th International Conference on Informatics and Systems (INFOS), Cairo, Egypt

Badakhshannoory, H., & Saeedi, P. (2011). A model-based validation scheme for organ segmentation in CT scan volumes. *Institute of Electrical and Electronics Engineers Transaction on Biomedical Engineering, 58*(9), 2681-2693. doi: 10.1109/tbme.2011.2161987

Bartnykas, K. (2010). Segmentation of liver region based on multifractal analysis. *Electronics and Electrical Engineering*, *2*(98), 79-82.

Gao, L., Heath, D. G., Kuszyk, B. S., & Fishman, E. K. (1996). Automatic liver segmentation technique for three-dimensional visualization of CT data. *Radiology*, *201*(2), 359-364.

Hori, M., Suzuki, K., Epstein, M. L., & Baron, R. L. (2011). Computed tomography liver volumetry using 3-dimensional image data in living donor liver transplantation: effects of the slice thickness on the volume calculation. *Liver Transplantation*, *17*(12), 1427-1436.

Huang, S. -h., Wang, B. -l., Cheng, M., Wu, W. -l., Huang, X. -y., & Ju, Y. (2008). A fast method to segment the liver according to Couinaud's classification. In X. Gao, H. Müller, M. Loomes, R. Comley, & S. Luo (Eds.), *Medical imaging and informatics* (Vol. 4987, pp. 270-276). Berlin, Germany: Springer

Jiang, H., He, B., Fang, D., Ma, Z., Yang, B., & Zhang, L. (2013). A region growing vessel segmentation algorithm based on spectrum information. *Computational and Mathematical Methods in Medicine*, 743-870

Lesage, D., Angelini, E. D., Bloch, I., & Funka-Lea, G. (2009). A review of 3D vessel lumen segmentation techniques: Models, features and extraction schemes. *Medical Image Analysis*, 13(6), 819-845.

Liu, F., Zhao, B., Kijewski, P. K., Wang, L., & Schwartz, L. H. (2005). Liver segmentation for CT images using GVF snake. *Medical Physics*, *32*(12), 3699-3706.

Masood, A., & Ejaz, S. (2010). An efficient algorithm for robust curve fitting using cubic Bezier curves. In D. -S. Huang, X. Zhang, C. Reyes García, & L. Zhang (Eds.), *Advanced intelligent computing theories and applications. With aspects of artificial intelligence* (Vol. 6216, pp. 255-262). Berlin, Germany: Springer

Oliveira, D. A., Feitosa, R. Q., & Correia, M. M. (2011). Segmentation of liver, its vessels and lesions from CT images for surgical planning. *Biomedical Engineering Online*, *10*(1), 1-23.

Rutkauskas, S., Gedrimas, V., Pundzius, J., Barauskas, G., & Basevicius, A. (2006). Clinical and anatomical basis for the classification of the structural parts of liver. *Medicina (Kaunas), 42*(2), 98-106.

Sato, Y., Nakajima, S., Shiraga, N., Atsumi, H., Yoshida, S., Koller, T., . . . Kikinis, R. (1998). Three-dimensional multi-scale line filters for segmentation and visualization of curvilinear structures in medical images. *Medical Image Analysis*, *2*(2), 143-168.

Suzuki, K., Epstein, M. L., Kohlbrenner, R., Garg, S., Hori, M., Oto, A., & Baron, R. L. (2011). Quantitative radiology: Automated CT liver volumetry compared with interactive volumetry and manual volumetry. *American Journal Roentgenology, 197*(4), W706-712. doi: 10.2214/ajr.10.5958.

Suzuki, K., Kohlbrenner, R., Epstein, M. L., Obajuluwa, A. M., Xu, J., & Hori, M. (2010). Computer-aided measurement of liver volumes in CT by means of geodesic active contour segmentation coupled with level-set algorithms. *Medical Physics*, *37*(5), 2159-2166.

Xu, Y., Liu, Z., & Ji, L. (2010, October). *Liver CT image segmentation by local entropy method.* Paper presented at the International Conference on Computer Application and System Modeling (ICCASM), 2010.

Yi, J., & Ra, J. B. (2003). A locally adaptive region growing algorithm for vascular segmentation. *International Journal of Imaging Systems and Technology*, *13*(4), 208-214.